

Provided for non-commercial research and education use.
Not for reproduction, distribution or commercial use.



This article appeared in a journal published by Elsevier. The attached copy is furnished to the author for internal non-commercial research and education use, including for instruction at the authors institution and sharing with colleagues.

Other uses, including reproduction and distribution, or selling or licensing copies, or posting to personal, institutional or third party websites are prohibited.

In most cases authors are permitted to post their version of the article (e.g. in Word or Tex form) to their personal website or institutional repository. Authors requiring further information regarding Elsevier's archiving and manuscript policies are encouraged to visit:

<http://www.elsevier.com/copyright>



Contents lists available at ScienceDirect

Composites: Part A

journal homepage: www.elsevier.com/locate/compositesaFoam processing of polyethylene ionomers with supercritical CO₂Tomoki Mori^a, Hidetomo Hayashi^a, Masami Okamoto^{a,*}, Satoshi Yamasaki^b, Hiroshi Hayami^b^aAdvanced Polymeric Nanostructured Materials Engineering, Graduate School of Engineering, Toyota Technological Institute, Hisakata 2-12-1, Tempaku, Nagoya 468-8511, Japan^bPolymer Materials Technology R&D, Department Electronics & Materials R&D Laboratories, Sumitomo Electric Industries, Ltd., Shimaya, Konohana-ku, 1-1-3, Osaka 554-0024, Japan

ARTICLE INFO

Article history:

Received 7 April 2009

Received in revised form 29 July 2009

Accepted 7 August 2009

Keywords:

Ionomer

Nano-structures

Foams

Rheological properties

ABSTRACT

Via a batch process, the foam processing of polyethylene-based ionomers having two different degree of the neutralization has been conducted using supercritical CO₂. The cellular structures obtained from various ranges of foaming temperature-CO₂ pressure were investigated by using field emission scanning electron microscopy. For comparison, the corresponding nano-composite also has been examined. The ionic cross-linked structure in the ionomer exhibited significant contribution to retard the cell growth and coalescence of cell, especially in ionomer having higher degree of the neutralization. For nano-composite foaming, experimentally, nano-clay particles led to an increase in cell density after foaming. However, the dispersed nano-clay particles did not act as nucleating sites for cell formation. The competitive phenomenon between the cell nucleation and the cell growth including the coalescence of cell was discussed in the light of the interfacial energy and the relaxation rate as revealed by the modified classical nucleation theory and rheological measurement, respectively.

© 2009 Elsevier Ltd. All rights reserved.

1. Introduction

About 30 years ago, Martini [1] first reported microcellular polymeric foams by using carbon dioxide (CO₂) as a physical-blowing agent. The microcellular foams are closed-cell morphology with a cell density in excess of 10⁸ cells/cm³ and cell diameter in the order of 10 μm. The rationale is that if the cell size is smaller than the critical flaws, which already exist in the bulk polymer matrix could be introduced in sufficient numbers, then the material density could be reduced while maintaining the essential mechanical properties. According to this method, the polymer is saturated with a gas or supercritical CO₂ at constant temperature and pressure. Then, the system is brought to the surer saturated state either by reducing pressure (pressure induced phase separation) or by increasing temperature (temperature induced phase separation) resulting in the nucleation and growth of pores (cells) inside the polymer matrix [2].

In our previous paper [3,4], we have devoted to study on evaluation of polymeric nano-composites in foam application. The incorporation of nano-clay induced heterogeneous nucleation because of a lower activation energy barrier compared with homogeneous nucleation as revealed by the characterization of the interfacial tension between bubble and matrix. Accordingly, nano-composites provided excellent foam having high cell density ($\geq 10^{13}$ cells/cm³) at low temperature with high CO₂ pressure condition, suggesting that the dispersed nano-clay particles act as

nucleating sites for cell formation and lowering of cell size (~200 nm). However, there are still some controversial data regarding the nucleating effect of the dispersed nano-clay particles.

Development of nano-composite foams is one of the latest evolutionary technologies of the polymeric foams. The nano-composite foams offer attractive potential for diversification and application of conventional polymeric materials. More detailed surveys on various types of nano-composite foaming can be also available in the literatures [5–8].

In the foaming process, the bubble growth is controlled by the gas diffusion from the matrix polymer into the cells, the melt viscosity of the material and overall pressure drop [2]. To study the above-mentioned effects on the obtainable morphological and mechanical properties of the nano-composite foams, it is necessary to select the materials having a wide range of melt viscosity. Accordingly, either nucleation effects or rheological effects should induce the intended differences in morphology.

Ionomers consist of random copolymer of ethylene and methacrylic acid (MA) where some of the acid groups are neutralized to form metal (sodium, zinc or magnesium) states [9]. Typically, the MA content of the copolymer is low (<15 mol%), and the degree of neutralization ranges from 20% to 60%. The incorporation of the ionic groups improves the toughness, melt viscosity, clarity, adhesion properties of the copolymer [9]. In addition, the ionic cross-linked (network) structure also may offer the possibility of favorable retardation effect on the cell growth and coalescence of cell during foaming.

To the best of our knowledge, the foaming of ionomers with supercritical CO₂ is not very well explored in literatures. Therefore,

* Corresponding author.

E-mail address: okamoto@toyota-ti.ac.jp (M. Okamoto).

we have attempted to investigate the correlation between foamability and melt rheology of polyethylene-based ionomers having different degree of the neutralization and corresponding nano-composite *via* a batch process in an autoclave. The ionic cross-linked structure in the ionomer expects significant contribution to retard the cell growth and coalescence of cell, especially in ionomer having higher degree of the neutralization.

2. Experimental

2.1. Materials

An ionomer resin (Himilan 1706: MA content = 15 wt.%, zinc oxide (ZnO) content = 3.70 wt.%, neutralization = ~55% and melt flow index (MI) = 4.1 g/10 min) purchased from Du Pont-Mitsui Polychemicals Co., Ltd., was used as a polymer matrix. The corresponding nano-composite, as a reference sample, was prepared by melt extrusion. The details of the nanocomposites preparation were described in our previous paper [10]. The abbreviations of two ionomers and the corresponding nano-composite also are presented in Table 1. The degree of neutralization is controlled by using ZnO (3 phr) and dodecyl tri-methyl ammonium chloride (as a neutralizing catalyst) [10].

2.2. Foam processing

The foam processing was conducted on ionomer 0/55, 0/89 and ionomer/clay 20/58 in an autoclave (TSC-WC-0096, Taiatsu Techno Co) by using supercritical CO₂ [4]. Basically, the physical foam processing (batch process) used in this study consists of three stages: (1) CO₂ saturation in the sample at desired temperature; (2) cell nucleation when the release of CO₂ pressure started (supersaturated CO₂) and cell growth to an equilibrium size during the release of CO₂; and (3) cell stabilization *via* cooling process of the foamed system. In the first stage, the specimen (10 × 20 × 0.9 mm³ = width × length × thickness) was inserted into an autoclave (96 mL) and CO₂ pressure was increased up to 30 MPa at various temperatures. Setup of the autoclave and temperature–pressure protocol used in this study is shown in Fig. 1. The temperature inside the autoclave was increased and maintained at a predetermined temperature using a band heater for temperature control. In this study, we conducted the experiments at three different foaming temperatures (*t_f*) (80–100 °C), just around melting temperature (~88 °C) of ionomer. The sample in the autoclave was heated from room temperature to *t_f* in 0.5 h to achieve the equilibrium state, and then dissolved in CO₂ for 5 h under the pressure range between 14 and 30 MPa. For such a long time of CO₂ dissolution into the sample, CO₂ has already been saturated in the sample at fixed *T_f*. In the second stage, the CO₂ pressure was rapidly reduced (within 3 s) in order to supersaturate the specimen with CO₂ gas [4]. The thermodynamic instability resulted in the formation of a large number of cell nuclei. After releasing the CO₂ pressure, the formed foams were stabilized *via* cooling by liquid-CO₂ to room temperature, and then removed carefully from the autoclave and kept at ambient temperature.

Table 1
Composition and characteristic parameter of ionomers and nano-composite.

Samples	Neutralization ^b (%)	Organo-clay (%)
Ionomer 0/55	55	0
Ionomer 0/89 ^a	89	0
Ionomer/clay 20/58	55	20

^a The sample is prepared using ZnO and dodecyl tri-methyl ammonium chloride.

^b The value measured by titrimetric analysis.

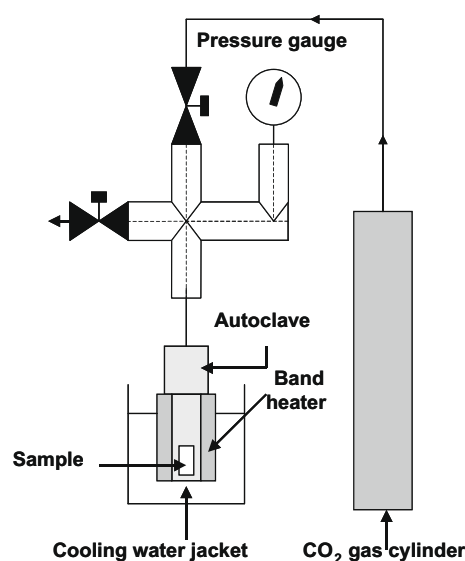


Fig. 1. Schematic representation of autoclave setup.

The cell structures were investigated by using field emission scanning electron microscope (FE-SEM) (S-4700, Hitachi Co.). The samples were freeze-fractured in liquid nitrogen and sputter-coated with platinum at an argon pressure of 0.1 Torr for 1.5 min at a current of 10 mA. The average cell radius (*d*) and the mean cell wall thickness (*δ*) were determined from the data of FE-SEM observation. The function for determining cell density (*N_c*) in cell/cm³ is defined as the following equation [3]:

$$N_c = \left[\frac{n}{A} \right]^{3/2} \quad (1)$$

where *n* is the number of cells in the area (*A*) of micrograph. The mass density of both pre-foamed (*ρ_p*) (=0.998 g/cm³) and post-foamed (*ρ_f*) in g/cm³ samples were estimated by using the buoyancy method [4].

2.3. Characterization

2.3.1. Differential scanning calorimetry (DSC)

The crystallized specimens were characterized by using temperature-modulated DSC (TMDSC) (TA 2920; TA Instruments) at the heating/cooling rate of 5 °C/min with a heating/cooling cycle of the modulation period of 60 s and an amplitude of 0.769 °C, to determine the crystallization temperature with cooling from melt (*T_c*), the melting temperature (*T_m*) and heat of fusion (*H*), the DSC was calibrated with indium before experiments.

2.3.2. Transmission electron microscopy (TEM)

Nanoscale structure of ionomer 0/55 was investigated by means of TEM (H-7100, Hitachi Co.), operating at an accelerating voltage of 100 kV. The ultra thin sections (the edge of the sample sheet perpendicular to the compression mold) with a thickness of 80 nm were microtomed at –80 °C using a Reichert Ultra cut cryo-ultramicrotome without staining. The number of ionic aggregated domains, consisting of Zn²⁺, in the micrograph was determined by the software.

2.3.3. Melt rheology

Melt rheological measurements were conducted on a RDAII instrument with a torque transducer capable of measurements in the range of 0.2–200 g cm. Dynamic oscillatory shear measurements were performed by applying a time dependent strain of

$\gamma(t) = \gamma_0 \sin(\omega t)$ and the resultant shear stress is $\sigma(t) = \gamma_0 [G' \sin(\omega t) + G'' \cos(\omega t)]$, with G' and G'' being the storage and loss modulus, respectively. Measurements were conducted by using a set of 25 mm diameter parallel plates with a sample thickness of ~ 1.0 mm and in the temperature range of 100–180 °C. The strain amplitude was fixed to 10% to obtain reasonable signal intensities even at elevated temperature or low frequency (ω) to avoid the nonlinear response. For each sample investigated, the limits of linear viscoelasticity were determined by performing strain sweeps at a series of fixed ω s. The master curves were generated using the principle of time–temperature superposition and shifted to a common reference temperature (T_r) of 100 °C, which was chosen as the most representative of a typical processing temperature of ionomer.

3. Results and discussion

3.1. Ionomer-based nano-composites formation

Fig. 2 shows the TMDSC thermograms of ionomer 0/55 and 0/89 and during heating from -50 °C, cooling from melt state (~ 190 °C) and second heating at a rate of 5.0 °C/min. For ionomer 0/55, the evolution of the crystallization peak is sharp and its maximum is at 55.25 °C. For ionomer 0/89, the peak is much broader and it appears at 48.40 °C. In addition, the ionomer exhibits lower total endothermic H (second heating) as compared with that of ionomer 0/55. The crystallization of ionomer 0/89 is disturbed presumably due to the effect of the large degree of the neutralization (i.e., ionic cross-linked density). In first run, small peaks around 50 °C correspond to the thermally unstable crystals such as the poor chain packing or disordered crystals, which are depended on the thermal history.

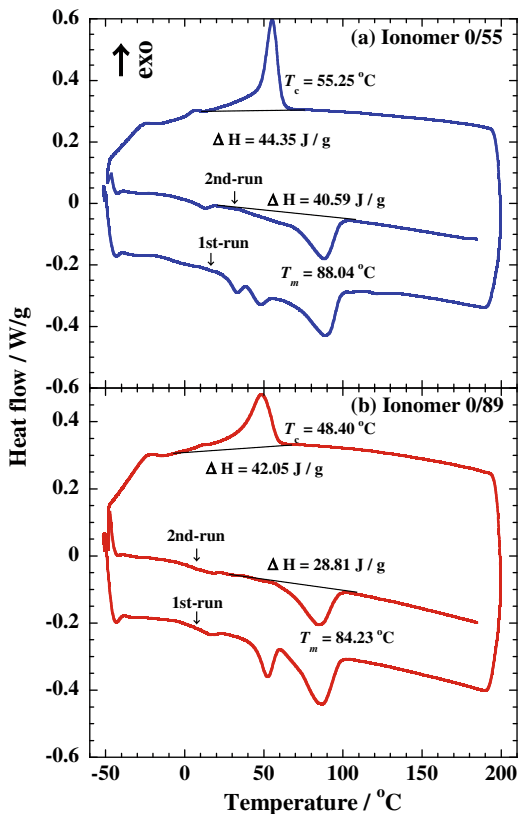


Fig. 2. TMDSC scan for (a) ionomer 0/55 and (b) ionomer 0/89.

3.2. Morphology of ionomer foams

Fig. 3 shows the typical results of FE-SEM images of the fracture surfaces of the ionomers foamed at a temperature range of 80–100 °C under the different isobaric saturation conditions (14, 22 and 30 MPa). All foams exhibit nicely the closed-cell structure. We noted here that homogeneous cells were formed in case of ionomer 0/89 foams, while ionomer 0/55 foams show rather non-uniform cell structure having large cell size. The ionomer 0/89 foams show smaller cell size and larger cell density compared with ionomer 0/55 foams, suggesting that the melt viscosity and modulus in ionomer 0/89 have some contribution to retard the cell growth and coalescence of cell during foaming. This feature will be discussed later. For both foam systems, we have calculated the distribution function of cell size from the FE-SEM images and the results are presented in Fig. 4. The ionomer foams nicely obeyed the Gaussian distribution. In case of ionomer 0/89 foamed at 90 °C under high pressure of 26 MPa, we can see that the width of the distribution peaks, which indicates the cell size distribution, became narrow accompanied by the large degree of the neutralization (89%).

From the FE-SEM images, we have quantitatively calculated various morphological parameters of two different foam systems.

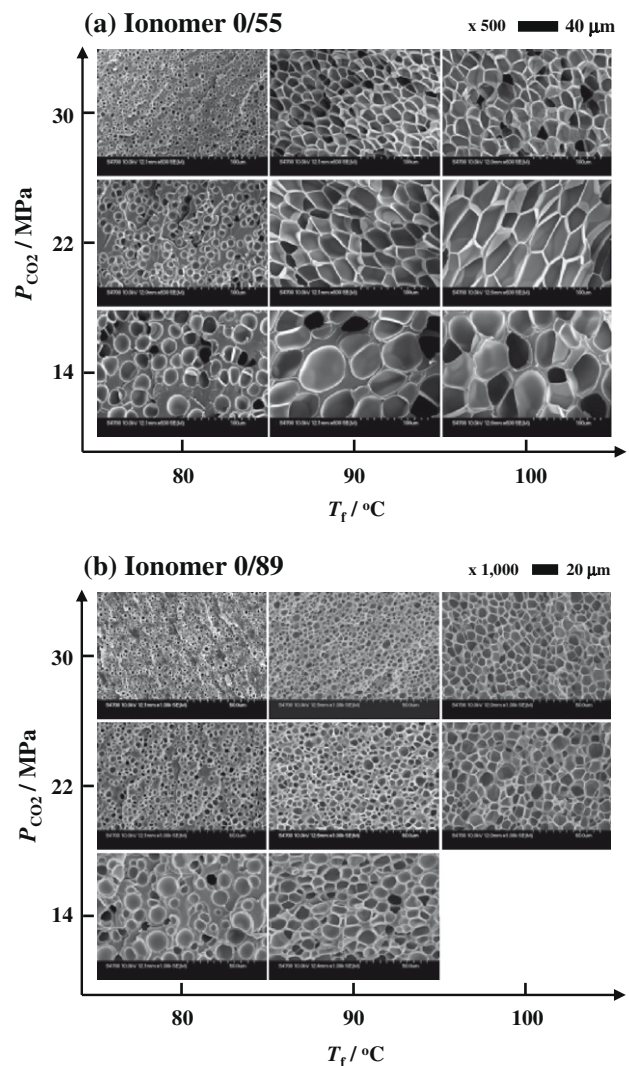


Fig. 3. Typical results of FE-SEM images of the fracture surfaces of (a) ionomer 0/55 and (b) ionomer 0/89 foamed at temperature range of 80–100 °C under different isobaric saturation condition (14, 22 and 30 MPa).

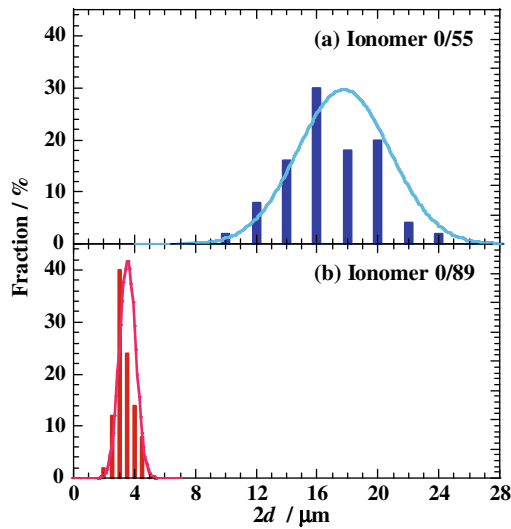


Fig. 4. Typical example for cell size distribution of foamed (a) ionomer 0/55 and (b) ionomer 0/89 in experiment at 90 °C under 26 MPa. Average values $2d$ in μm and standard deviation σ_d in m in the Gaussian fit through the data are 17.7 and 3.04 for ionomer 0/55 and 3.55 and 0.54 for ionomer 0/89 foams, respectively.

At high foaming temperature ($T_f \sim 100\text{ }^\circ\text{C}$), both systems exhibit the polygon closed-cell structures having pentagonal and hexagonal faces, which express the most energetically stable state of polygonal cells. Such foam structure was obtained probably because these foams belong to the polymeric foams having high gas phase volume (>0.7) [11] (see Fig. 5).

Obviously, with decreasing saturation pressure condition ($\sim 80\text{ }^\circ\text{C}$ and 14 MPa), both systems exhibit large cell size due to the low supply of CO_2 molecules, which can subsequently form a

small population of cell nuclei upon depressurization [4]. However, the competition between homogeneous and heterogeneous nucleation is no longer discernible. This phenomenon will be discussed later.

3.3. Foaming pressure dependence of cellular structure

The dependence of the density ratio (ρ_f/ρ_p) at three T_f s under different CO_2 pressure is shown in Fig. 5. For ionomer 0/55, throughout the whole T_f range, the mass density of the foams shows gradual decrease with increasing CO_2 pressure. At high T_f ($\sim 100\text{ }^\circ\text{C}$), the mass density is rapidly reduced and then attains a minimum constant value up to 30 MPa as compared with that of low T_f condition ($\sim 80\text{ }^\circ\text{C}$). On the other hand, for ionomer 0/89, we can observe weak pressure dependence of ρ_f/ρ_p , suggesting the high viscosity of the matrix ionomer 0/89 owing to the high ionic cross-linked density caused by the large degree of the neutralization. From the above results, it can be said that such behavior of mass density is due to the competition between the cell nucleation and the cell growth. At the low T_f range ($\sim 80\text{ }^\circ\text{C}$), in which a large supply of CO_2 molecules are provided, the cell nucleation is dominant, while at the high T_f ($\sim 100\text{ }^\circ\text{C}$), the cell growth and the coalescence of cell are prominent due to low viscosity of the systems compared with the low T_f range ($\sim 80\text{ }^\circ\text{C}$) [4]. This behavior clearly appears in the plots of the cell size ($\cong 2d$), the cell density (N_c), and the mean cell wall thickness (δ) versus CO_2 pressure at various T_f conditions, respectively. As seen in Fig. 6, we find that with increasing CO_2 pressure two ionomer foams show an increasing tendency of N_c and attain a maximum in case of ionomer 0/89 with high T_f condition ($\sim 100\text{ }^\circ\text{C}$). On the other hand, the pressure dependence of $2d$ and/or δ shows opposite behavior compared with the tendency of N_c due to the cell nucleation (see Figs. 7 and 8). Both $2d$ and N_c affect the mass density of the foams.

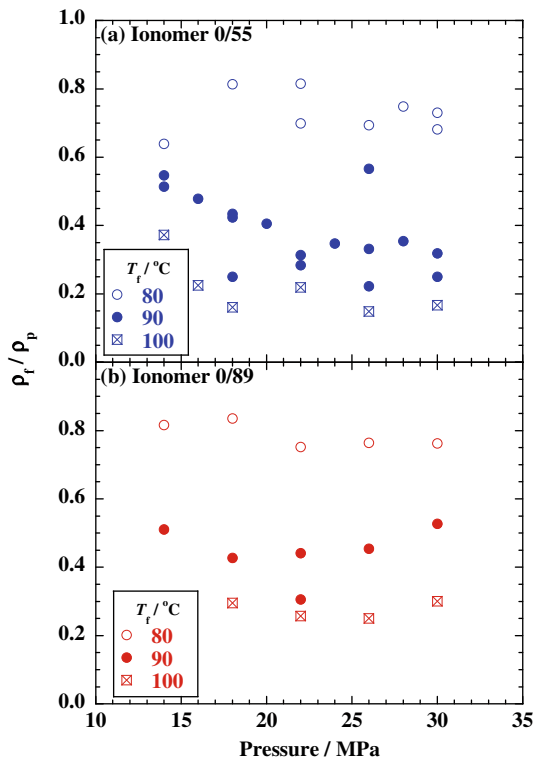


Fig. 5. CO_2 pressure dependence of the density ratio $\frac{\rho_f}{\rho_p}$ for (a) ionomer 0/55 and (b) ionomer 0/89 foamed at three different T_f s.

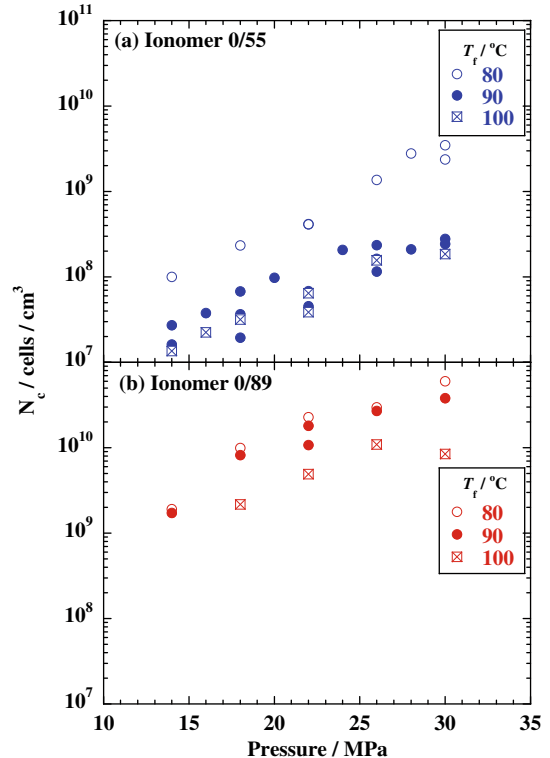


Fig. 6. CO_2 pressure dependence of the cell density (N_c) for (a) ionomer 0/55 and (b) ionomer 0/89 foamed at three different T_f s.

In Figs. 9 and 10, we show the relations between $2d$ and N_c , and δ and $2d$ in this study. The relations nicely obey in ($2d \sim N_c^{-1/3}$) and ($\delta \sim 2d^1$). The ionomer 0/89 foams enhance the value of N_c accompanied with the small value of δ as compared with that of ionomer 0/55 foams. In case of ionomer foams, the controlled structure is from $2d \cong 5\text{--}40\text{ m}$ with $N_c \cong 10^7\text{--}10^9\text{ cells cm}^{-3}$ for ionomer 0/55 to $2d \cong 1\text{--}10\text{ m}$ with $N_c \cong 10^9\text{--}10^{11}\text{ cells cm}^{-3}$ for ionomer 0/89, respectively.

3.4. Theoretical correlations

We conducted the characterization of the interfacial tension between bubble and matrix by using the modified classical nucleation theory [12].

According to the theory proposed by Suh and Colton, the rate of nucleation of cells per unit volume (\dot{N}) can be written as

$$\dot{N} \sim Cf \exp \left[\frac{-16\pi\gamma^3 S(\theta)}{3(\Delta P_{CO_2})^2 k_B T} \right] \quad (2)$$

where C is the concentration of CO_2 and/or the concentration of heterogeneous nucleation sites, f is the collision frequency of CO_2 , γ is the interfacial tension between bubble and matrix, $S(\theta)$ is the energy reduction factor for the heterogeneous nucleation, ΔP_{CO_2} is the magnitude of the pressure quench during depressurization, k_B is the Boltzmann constant, and T is absolute temperature.

The theoretical cell density is given by

$$N_{theor} = \int_0^t \dot{N} dt \quad (3)$$

where t is the foaming time that takes approximately 3 s.

Generally we can observe the cumulative number of cell and apparent pressure quench depth. For this reason, our characterization of the interfacial tension is obtained from a rough approximation.

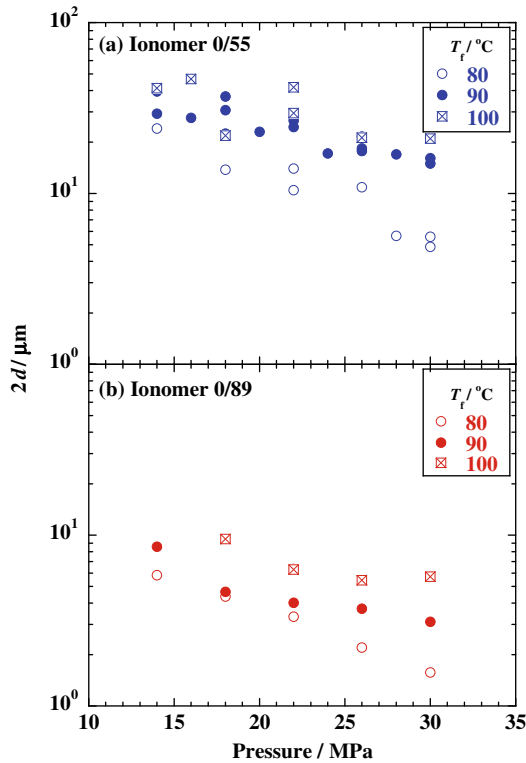


Fig. 7. CO_2 pressure dependence of the mean cell wall thickness (δ) for (a) ionomer 0/55 and (b) ionomer 0/89 foamed at three different T_f s.

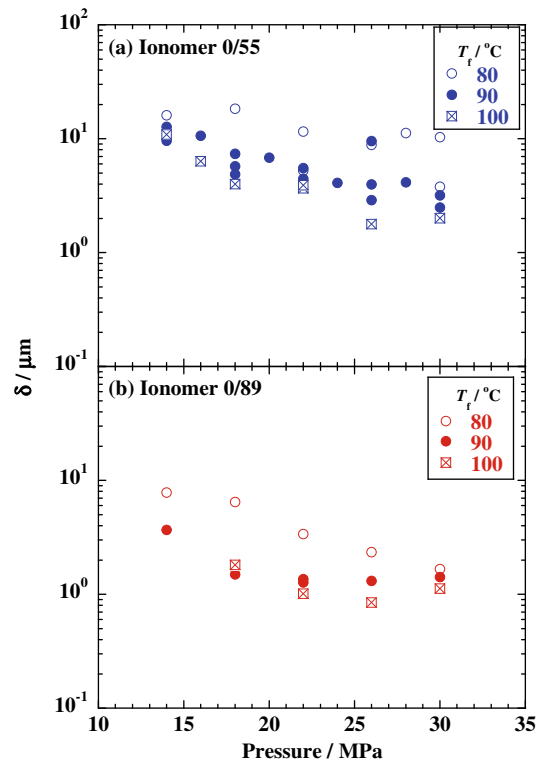


Fig. 8. CO_2 pressure dependence of the cell size ($\cong 2d$) for (a) ionomer 0/55 and (b) ionomer 0/89 foamed at three T_f s.

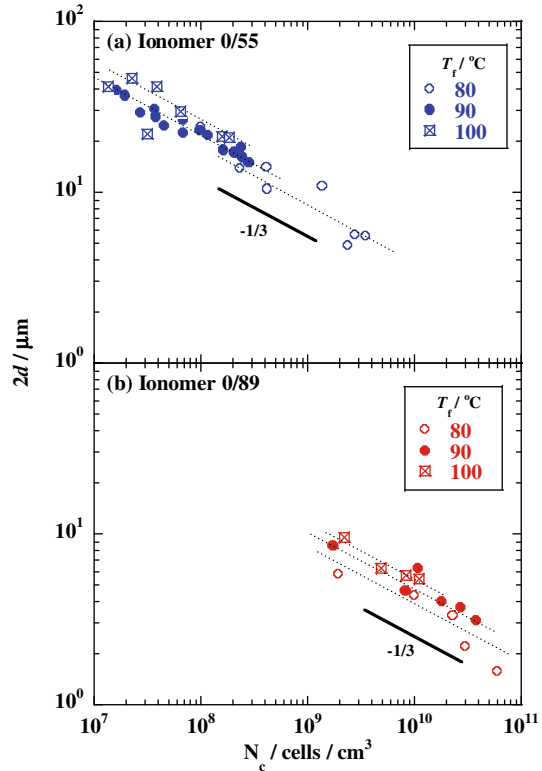


Fig. 9. Relation between cell size versus cell density for all ionomer foams. The dashed line indicates the slope $-1/3$.

We consider here the effect of the pressure drop rate on the cell nucleation. An increase in pressure drop rate leads to the appearance

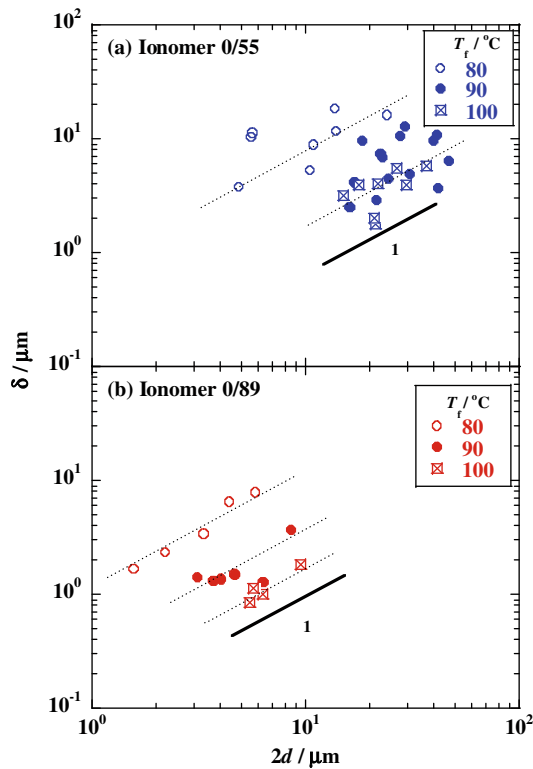


Fig. 10. Relation between cell wall thickness versus cell size for all ionomer foams. The dashed line indicates the slope 1.

of a large number of nucleated cells as compared with the slower pressure drop (~ 14 MPa). For slower pressure drops the cell diameter but not the number of first formed cell increases. At the same time, under the increasing saturation condition (~ 30 MPa) we have to take the effect of the residue of CO_2 on the viscosity of the materials into consideration. For this reason the situation is very complex to explain well. This discussion is beyond the objective of this paper, and we will report separately.

At the low T_f (80 °C), the value of N_c decreases with ΔP_{CO_2} (~ 14 –30 MPa) because the cell growth is prominent. Assuming no effect of the coalescence of cell on the value of N_c , we estimate the interfacial energy ($S(\theta)^{1/3}$) of the systems calculated using Eqs. (2) and (3), i.e., the slope of the plots (N_c versus $1/\Delta P_{\text{CO}_2}^2$). For all cases examined the plots conform to the straight lines (see Fig. 11) as predicted by Eqs. (2) and (3). For comparison, we also show the result of ionomer/clay 20/58 foamed at 90 °C (see Appendix A). The characteristic parameters of three systems are also summarized in Table 2. The evaluated result gives almost same value (~ 6 mJ/m²) and does not depend on the processing temperature and systems. The estimated values are good agreement with that of other polymer- CO_2 system (~ 10 mJ/m²) [4,12]. However, the nano-composite (ionomer/clay 20/58) foams exhibit smaller cell size and larger cell density without the significant difference in $\gamma S(\theta)^{1/3}$ as compared with neat ionomer 0/55 foams, suggesting that the dispersed silicate particles do not act as nucleating sites for cell formation. This trend reflects the relative importance of the cell growth and the coalescence of cell. That is, we have to take the viscosity effect (relaxation time) on the cell coalescence of cell into consideration.

3.5. Melt rheology and relaxation time

To confirm the viscosity effect on the cell coalescence we investigated the flow behavior of the ionomers and the corresponding

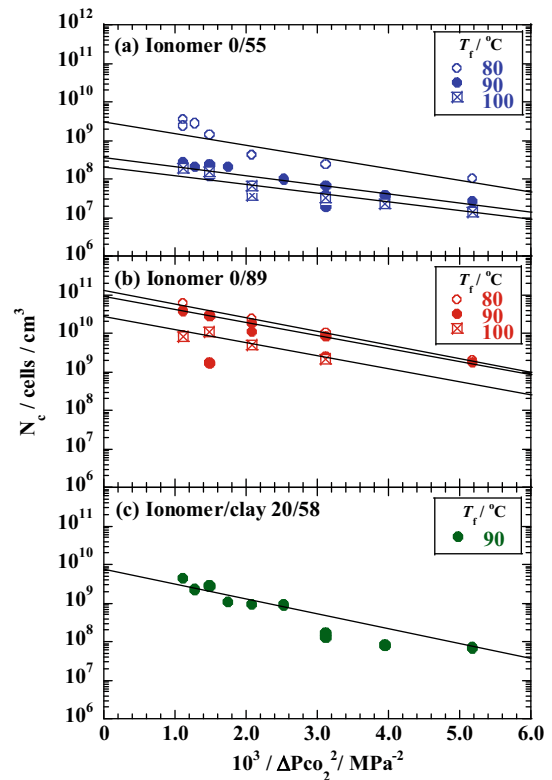


Fig. 11. Plots of cell density (N_c) versus reciprocal CO_2 pressure $1/(P_{\text{CO}_2})^2$ for (a) ionomer 0/55, (b) ionomer 0/89 and (c) ionomer/clay 20/58 foamed at different T_f .

Table 2
Characteristic interfacial parameter of three systems at different T_f .

Systems	T_f (°C)	$\gamma S(\theta)^{1/3}$ (mJ/m ²)
ionomer 0/55	80	6.1
	90	5.2
	100	5.7
ionomer 0/89	80	6.2
	90	6.1
	100	6.7
ionomer/clay 20/58	90	6.7

nano-composite (see Fig. 12). The slope of $G'(\omega)$ and $G''(\omega)$ versus the $a_T\omega$ is much smaller than 2 and 1, respectively. Values of 2 and 1 are expected for linear mono-dispersed polymer melts, and are large deviation may be due to the formation of the ionic cross-linked network structure in the melt state [10] (see Appendix B). The temperature dependence frequency shift factor (a_T , Arrhenius-type) is used to generate master curves shown in Fig. 12. To understand the generic dynamic rheology, the cross over frequency ω_{rel} in the master curve of the dynamic frequency sweep enables one to predict a relaxation time ($=1/\omega_{\text{rel}}$), which is determined from the measured master curve when $\tan \delta$ is unity. Fig. 13 shows the results of the temperature dependence of relaxation rate (ω_{rel}), assuming that the rate is of Arrhenius-type.

For ionomer 0/89, the estimated relaxation rates are about 0.082–12.5 s⁻¹ in the range of temperature between 100 °C and 180 °C. These values are much smaller than those of ionomer 0/55 (those are in fact 0.24–84.5 s⁻¹), suggesting the ionic cross-linked density (the degree of the neutralization) is dominant factor for the relaxation time scale. The slope that reflects the activation energy of each process exhibits different value. The activation energy of the relaxation process is also estimated (see Table 3). An

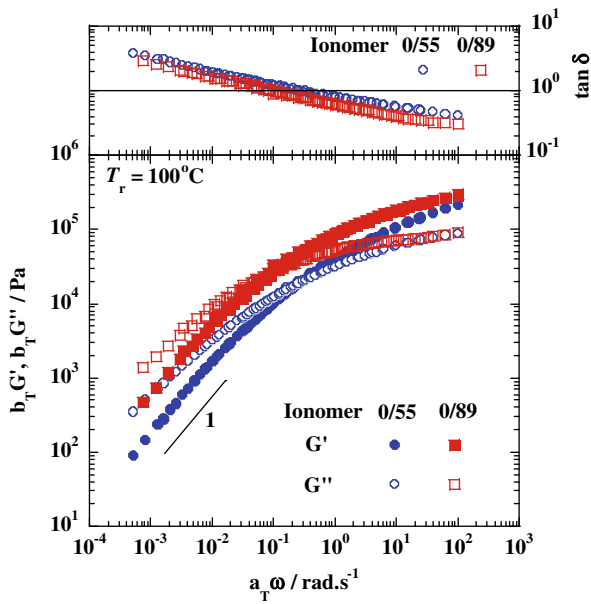


Fig. 12. Reduced frequency dependence of storage modulus $G'(\omega)$, loss modulus $G''(\omega)$ and $\tan \delta$ of ionomer 0/55 and 0/89 at $T_r = 100^\circ\text{C}$. $b_T = \rho T / \rho_r T_r$, where ρ and ρ_r are the density at T and T_r , respectively. The solid line was drawn by the power law of $G'(\omega) - G''(\omega) - \omega$ in the low ω region.

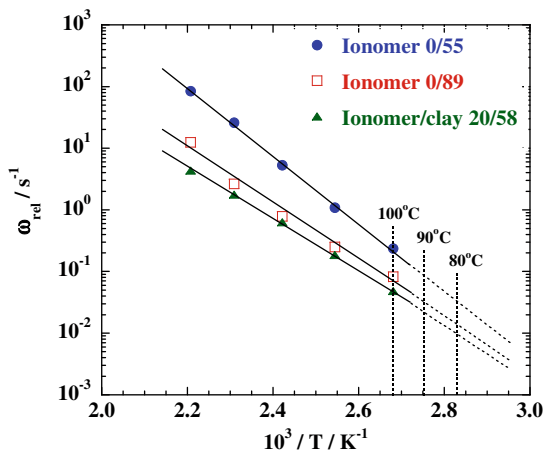


Fig. 13. Temperature dependence of characteristic relaxation rates (ω_{rel}) of ionomer 0/55, ionomer 0/89 and ionomer/clay 20/58. The foaming temperature range (80 °C, 90 °C and 100 °C) is shown.

interesting feature is that in the range of temperature between 80 °C and 100 °C this trend remains by extrapolation based on plotting ω_{rel} versus reciprocal temperature, $1/T$.

The ionic cross-linked structure has significant contribution to retard the cell growth and coalescence of cell. For this reason, ionomer 0/89 foams lead to large value of N_c accompanied with the small value of δ as compared with that of ionomer 0/55 foams. That is, in the ionomer foaming the cell coalescence is dominant factor

Table 3
Activation energy of each system.

Samples	E_a (kJ/mol)
Ionomer 0/55	104.9
Ionomer 0/89	86.6
Ionomer/clay 20/58	79.2

rather than the promoting heterogeneous nucleation. Meanwhile, ionomer/clay 20/58, a same feature is observed as well as ionomer 0/89 foaming, implying that the nucleating effect of the dispersed nano-clay particles is overwhelmed (i.e., no enhancement of the nucleation).

4. Conclusions

We have discussed foam processing of polyethylene-based ionomers having two different degree of the neutralization by using supercritical CO_2 as a physical foaming agent in a batch process at various temperatures and CO_2 pressure ranges. The ionic cross-linked structure exhibited significant contribution to retard

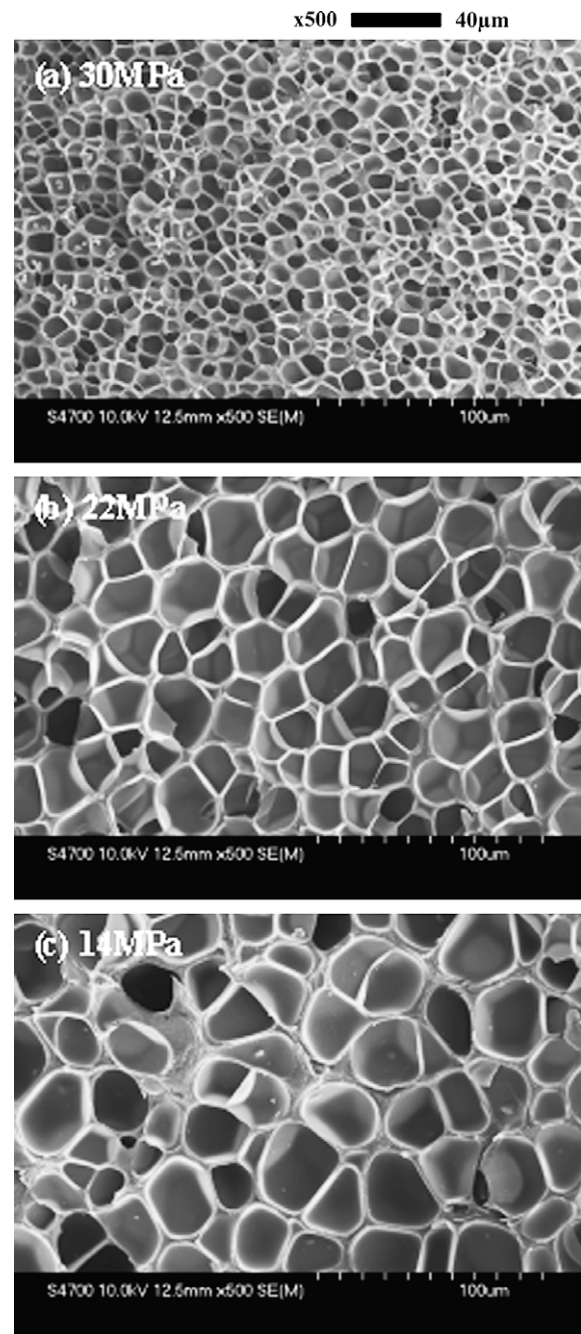


Fig. 14. Typical results of FE-SEM images of the fracture surfaces of the nano-composite foamed at a temperature range of 90 °C under the different isobaric saturation conditions (14, 22 and 30 MPa).

the cell growth and coalescence of cell. For this reason, the ionomer 0/89 foams enhanced the value of N_c accompanied with the small value of δ as compared with that of ionomer 0/55 foams. In case of ionomer foams, the controlled structure is from $2d \cong 5\text{--}40\ \mu\text{m}$ with $N_c \cong 10^7\text{--}10^9\ \text{cells cm}^{-3}$ for ionomer 0/55 to $2d \cong 1\text{--}10\ \mu\text{m}$ with $N_c \cong 10^9\text{--}10^{11}\ \text{cells cm}^{-3}$ for ionomer 0/89, respectively. For comparison, we have examined foam processing of ionomer-based nano-composite (ionomer/clay 20/58). Experimentally, nano-clay particles led to an increase in N_c . In the ionomer foaming the cell coalescence was dominant factor rather than the promoting heterogeneous nucleation. Meanwhile, ionomer/clay 20/55, a same feature was observed as well as ionomer 0/89 foaming. The nucleating effect of the dispersed nano-clay particles was overwhelmed (i.e., no enhancement of the nucleation).

Acknowledgment

This work was supported by the STAS Project (2005–2009).

Appendix A

A.1. Nano-composite foaming

For comparison, we conducted foam processing of ionomer/clay 20/58. Fig. 14 shows the typical results of FE-SEM images of the fracture surfaces of the nano-composite foamed at a temperature range of 90 °C under the different isobaric saturation conditions (14, 22 and 30 MPa) (cf. Fig. 3a). As seen in Figs. 15 and 16, the nano-composite foams show smaller cell size and larger cell density compared with neat ionomer 0/55 foams. Experimentally, nano-clay particles lead to an increase in N_c . However, we can not identify how do the dispersed nano-clay particles act as nucleating sites for cell formation?

Appendix B

B.1. Nanoscale structure of ionomer 0/55

Fig. 17 shows the results of TEM bright field images of ionomer 0/55. In Fig. 17, the dark areas represent the nano-sized ionic aggregates similar to what is observed for other ionomers [13]. After a close look we clearly observe spheres with a domain size (L) of approximately 2–3 nm (indicated with arrows). The ionic aggregates are randomly arranged in the ionomer matrix. The

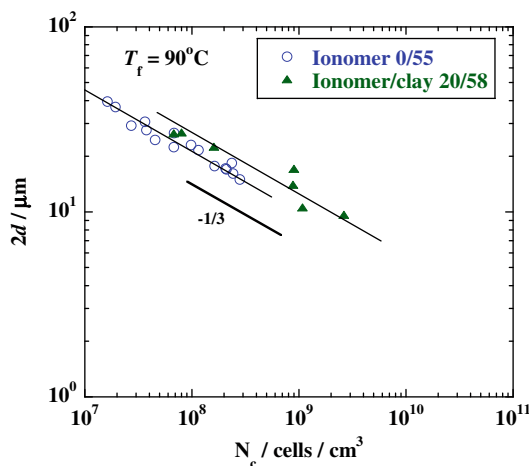


Fig. 15. Relation between cell size versus cell density for ionomer/clay 20/58 foam. The dashed line indicates the slope $-1/3$.

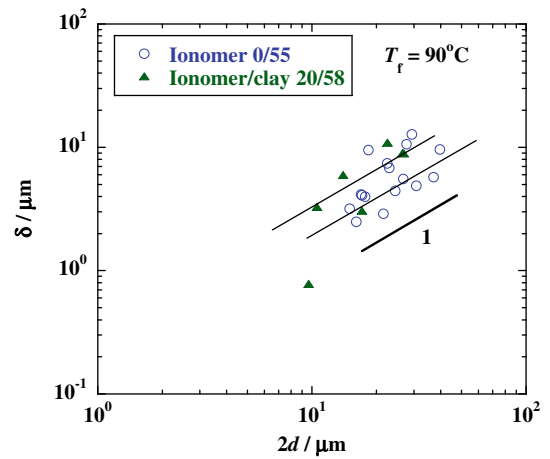


Fig. 16. Relation between cell wall thickness versus cell size for ionomer/clay 20/58 foam. The dashed line indicates the slope 1.

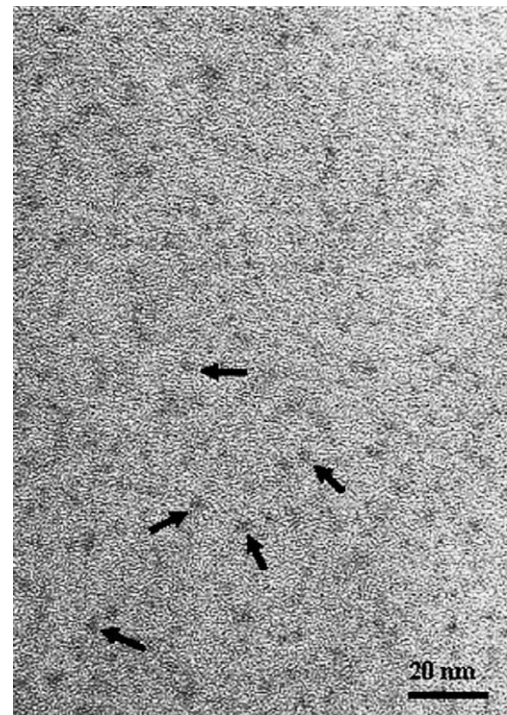


Fig. 17. Bright field TEM images of ionomer 0/55. The arrows indicate the nano-sized ionic aggregates in the original images. The bright areas are the matrix.

number of the aggregates (N_{ion}) can be estimated from the enlarged images. The calculated value of N_{ion} was $0.08\text{--}0.12\ \text{nm}^{-2}$ for ionomer 0/55.

In the heterogeneous nucleation, we have to take the reduction of the critical energy into consideration because of the inclusion of nucleants, which is a function of the ionomer-gas-inclusion contact angle (θ) and the relative curvature (W) of the nucleant surface to the critical radius of the nucleated phase [14].

The critical size of the nuclei generated at any condition can be calculated by [14]

$$r^* = 2\gamma/\Delta P_{CO_2} \tag{A1}$$

where r^* is the radius of the critical nuclei. Under this experimental condition, r^* is $\sim 1.0\ \text{nm}$.

The relative curvature ($W = L/2r^*$) are 1–1.5. In case of $W \leq 2$, the energy reduction factor ($S(\theta)$) does not depend on the contact angle. For this reason, we could not observe the inclusion effect on the heterogeneous nucleation, completely diminishing the benefit of the nano-sized ionic aggregates. The ionomers exhibit no significant difference in $S(\theta)^{1/3}$. This reasoning is consistent with the small value of W in both ionomer systems as expected.

References

- [1] Martini JE. Ph.D. Thesis, Massachusetts Institute of Technology, USA; 1981.
- [2] Kumar V, Suh NP. *Polym Eng Sci* 1990;30:1323–9.
- [3] Ito Y, Yamashita M, Okamoto M. *Macromol Mater Eng* 2006;291:773–83.
- [4] Ema Y, Ikeya M, Okamoto M. *Polymer* 2006;47:5350–9.
- [5] Lee LJ, Zeng C, Cao X, Han X, Shen J, Xu G. *Compos Sci Technol* 2005;65:2344–63.
- [6] Cao X, Lee LJ, Widya T, Macosko C. *Polymer* 2005;46:775–83.
- [7] Chandra A, Gong S, Turng LS, Gramann P, Cordes H. *Polym Eng Sci* 2005;45:52–61.
- [8] Strauss W, D'Souza NA. *J Cellular Plastics* 2004;40:229–41.
- [9] Eisenberg A, Kim JS. *Introduction to ionomers*. New York: Wiley; 1998.
- [10] Shigemori T, Okamoto M, Yamasaki S, Hayami H. *Composites: Part A* 2008;39:1924–9.
- [11] Nam PH, Okamoto M, Maiti P, Kotaka T, Nakayama T, Takada M, et al. *Polym Eng Sci* 2002;42:1907–18.
- [12] Colton JS, Suh NP. *Polym Eng Sci* 1987;27:485–92.
- [13] Lefelar JA, Weiss RA. *Macromolecules* 1984;17:1145–8.
- [14] Fletcher NH. *J Chem Phys* 1958;29:572–6.